Hindawi
Journal of Robotics
Volume 2020, Article ID 8571318, 11 pages
https://doi.org/10.1155/2020/8571318

Research Article

Stiffness and Elastic Deformation of 4-DoF Parallel Manipulator with Three Asymmetrical Legs for Supporting Helicopter Rotor

Jialin Song,[1] Yang Lu,[2] Yongli Wang,[3] and Yi Lu [3]

[1]*College of Electrical Engineering, Yanshan University, Qinhuangdao, Hebei 066004, China*
[2]*Harbin Electric Corporation (Qinhuangdao) Heavy Equipment Company Limited, Qinhuangdao, Hebei 066004, China*
[3]*College of Mechanical Engineering, Yanshan University, Qinhuangdao, Hebei 066004, China*

Correspondence should be addressed to Yi Lu; luyi@ysu.edu.cn

Received 21 July 2019; Revised 18 August 2019; Accepted 10 November 2019; Published 1 February 2020

Academic Editor: Gordon R. Pennock

The stiffness and elastic deformation of a 4-DoF parallel manipulator with three asymmetrical legs are studied systematically for supporting helicopter rotor. First, a 4-DoF 2SPS + RRPR type parallel manipulator with two linear SPS type legs and one RRPR type composite leg is constructed and its constraint characteristics are analyzed. Second, the formulas for solving the elastic deformation and the stiffness matrix of the above mentioned three asymmetrical legs are derived. Third, the formulas for solving the total stiffness matrix and the elastic deformation of this manipulator are derived and analyzed. Finally, its finite element model is constructed and its elastic deformations are solved using both the derived theoretical formulas and the finite element model. The theoretical solutions of the elastic deformations are verified by that of the finite element model.

1. Introduction

Various less mobility (less than 6-DoF) parallel manipulators (PMs) have been applied widely due to their merits, such as good performances in accuracy, rigidity, ability to manipulate large loads, and they are simple in structure and easy to control [1, 2]. Among them, some less mobility PMs with composite active constrained legs attract more attention because they have larger workspace, better flexibility and fewer legs for avoiding interferences easily; the unnecessary tiny self-movement can be eliminated by the composite active constrained legs; more actuators can be installed onto the base for reducing vibration [1, 2]. Therefore, this type of PMs have potential applications for supporting helicopter rotor, airplane operation simulator, parallel machine tools, micro manipulators, sensors, surgical manipulators, tunnel borers, barbettes of war ship, and satellite surveillance platforms. Stiffness is one of the important performances of PMs, because higher stiffness allows larger variable load and higher speeds with higher precision of the end-effector [3]. Therefore, it is significant to analyze the stiffness and to evaluate elastic deformation of this type of PMs in the early design stage. Let (R, P, U, S) be (revolute, prismatic, universal, spherical) joint, respectively. In this aspect, Gosselin and Zhang developed virtual joint method allowed taking into account the links flexibility, which were presented as rigid beams supplemented by linear and torsional springs [3]. Zhang and Lang Sherman [4] established a stiffness modeling for PMs with one passive leg. Dong et al. [5] analyzed the stiffness modeling and stiffness distributions of a 5-DOF hybrid robot by considering the component compliances associated with the elements of both the PM and the wrist. Li and Xu [6] derived stiffness matrix of a 3-PUU PM based on an overall Jacobian using the screw theory by considering the effect of actuations and constraints. Yang et al. [7] studied elastostatic stiffness modeling of over constrained PMs. Zhou et al. [8] derived the stiffness matrix of a redundantly actuated parallel mechanism based on the overall Jacobian. Based on strain energy and Castigliano's theorem, Enferadi and Tootoonchi [9] obtained mathematical model of the manipulator stiffness matrix. Pashkevich et al. [10] proposed a methodology to enhance the stiffness of serial and parallel manipulators with passive joints, the manipulator elements are presented as pseudo-rigid bodies separated by multidimensional virtual springs and perfect passive joints; they [11] also presented a stiffness modeling method for over-constrained PMs with flexible links and compliant actuating

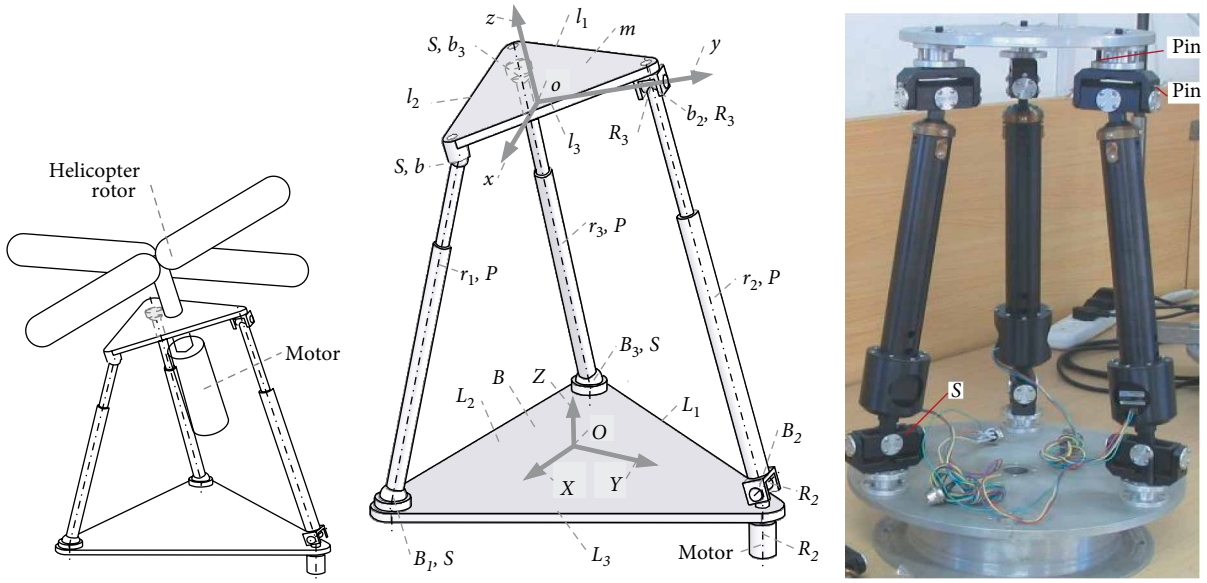

Figure 1: A 2SPS+RRPR PM for supporting helicopter rotor (a), 2SPS+RRPR type PM (b), and a prototype of reconfigurable 3SPS PM (c).

joints and the method of FEA-based link stiffness evaluation. Zhao et al. [12] deduced continuous stiffness matrix of a foldable PM for ship-based and the translation and rotational stiffness along any direction. Pham and Chen [13] established the stiffness model based on the way the flexure members are connected together in serial or parallel combinations. Chen et al. [14] derived a stiffness matrix of 3CPS PM based on the principle of virtual work considering the compliances subject to both actuators and legs. Shan et al. [15] established a overall stiffness model of the 2(3PUS+S) PM through a stiffness modeling method of a serial system. Hao and Kong [16] analyzed the mobility of spatial compliant multi-beam modules and derived their compliance matrices using a normalization technique. Wang et al. [17] investigated the stiffness characteristics of a hexaglide parallel loading machine, and derived its total stiffness matrix based on Jacobian matrix and statics. Lu et al. [18, 19] solved stiffness and elastic deformation for some less mobility PMs and serial-parallel manipulators by virtual mechanisms. Others [20–22] studied the stiffness and elastic deformation of PMs using above similar approaches and the virtual experiments in CAD environment. The above mentioned approaches for different PMs have their own merits. Since the above mentioned PMs are symmetrical in the structure and the distribution of active legs, the established stiffness matrices are symmetrical, and the elastic deformations of PMs can be solved more easily.

A 2SPS + RRPR type PM is a 4-DoF PM with three asymmetrical legs [23]. When the base of the 2SPS + RRPR type PM is fixed on top of the helicopter, and the rotor and its rotational actuator are installed on the moving platform of the 2SPS + RRPR type PM, the 2SPS + RRPR type PM can be used for the helicopter rotor supporter. Comparing with existing 4-DOF PM, the 2SPS + RRPR type PM has several merits as follows: (1) The stability and the capability of load bearing can be increased, the force situations can be improved, and the position workspace and the orientation workspace can be increased largely by rotating a revolute joint which connects the RRPR type composite leg with the base. (2) The unnecessary tiny self-movement can be removed and the precision can be increased using the RRPR type composite leg. (3) The number of oscillating legs is reduced, and the interference can be avoided easily. (4) The more actuators can be installed onto the base for reducing vibration.

Since the structure of the 2SPS + RRPR type PM is asymmetrical, it is a challenging and a significant issue to study the stiffness and elastic deformation of the 4-DOF PMs with asymmetrical structure by considering its constrained force. Therefore, this paper focuses on the study of the total stiffness and the elastic deformation of the 2SPS + RRPR PM by taking into account the elastic deformation due to constrained wrench. A finite element model of this PM is constructed for verifying the analytic solutions.

2. Kinematics and Statics of 2SPS + RRPR Type PM

A 2SPS + RRPR type PM for supporting helicopter rotor is shown in Figure 1(a). The 2SPS + RRPR PM is composed of a moving platform m, a fixed base B, and 2 SPS (spherical joint-active prismatic joint-spherical joint) type legs r_i (i = 1, 3) with the linear actuator, and one RRPR (active revolute joint- revolute joint -active prismatic joint-revolute joint) type composite active leg r_2 with a linear actuator and a rotational actuator, see Figure 1(b). Here, m is an equilateral ternary link $\Delta b_1 b_2 b_3$ with 3 sides $l_i = l$, 3 vertices b_i, and a center point o. B is an equilateral ternary link $\Delta B_1 B_2 B_3$ with 3 sides $L_i = L$, 3 vertices B_i, and a center point O. Each of $r_i (i = 1, 3)$ connects m to B by a spherical joint S at b_i, a leg r_i with active prismatic joint P, and S at B_i. The RRPR-type constrained composite active leg r_2 connects B to m by a universal joint U attached to B at B_2, a constrained leg r_2 with

active prismatic joint P, a revolute joint R_3 attached to m at b_2. The universal joint U at B_2 is composed of two cross revolute joints R_1 and R_2. Here, R_1 is connected with a rotational actuator. Therefore, the moving platform m of the 2SPS + RRPR type PM has 4 DOFs corresponding three rotations about R_1, R_1, R_1, and one translation along limb r_2. The degree of freedom of the 2SPS + RRPR type PM has been calculated and verified using its simulation mechanism in [23]. Since each of the SPS-type active legs $r_i (i = 1, 3)$ only bears the active force along r_i, it obviously has relative larger capacity of load bearing and is simple in structure. In addition, the unnecessary tiny self-movement of the 4-DoF 2SPS + RRPR PM can be eliminated effectively and its workspace can be enlarged by the RRPR-type constrained composite active leg r_2. Comparing with other 4-DOF PMs with four active legs, the 2SPS+RRPR PM with three active legs has merits as follows: (1) The interference among three active legs and the moving platform can be avoided easily. (2) Its whole mechanism is simplified. (3) Its moving platform provides more room for installing the helicopter rotor, finger mechanisms, tools.

A prototype of the reconfigurable 3SPS experimental model is built, see Figure 1(c). It includes a m, a B and 3 reconfigurable SPS-type legs $r_i (i = 1, 2, 3)$. Each of r_i connects B to m by a spherical joint S at B_i a reconfigurable leg r_i with active prismatic joint P, and S at b_i. Here, m and B are the same as that of the 2SPS+RRPR PM. Each of S joints is composed of three revolute joints R. It can be transformed into a U joint by adding one pin or be transformed into a R joint by adding two pins. Thus, the 2SPS + RRPR PM can be constructed easily from the prototype of reconfigurable 3SPS model to transform the upper S joint of r_2 into R joint by adding two pins, to transform the lower S joint of r_2 into U joint by adding one pin, and to add a rotational actuator onto the vertical revolute joint R_1 of U joint.

Let $\perp$ be a perpendicular constraint, $\|$ be a parallel constraint. Several geometric constraints (R_1 being coincident with the axis of motor, R_3 being coincident with y, $R_1 \| Z$, $R_1 \perp B$, $R_2 \perp R_1$, $R_2 \perp R_3$, $R_2 \perp r_2$ and $R_3 \perp r_2$) are satisfied in this PM. Let $\{m\}$ be a coordinate frame o-xyz fixed on m at o, $\{B\}$ be a coordinate frame O-XYZ fixed on B at O. Let (α, β, λ) be three Euler angles of m, φ be one of (α, β, λ). Set $s_\varphi = \sin\varphi$, $c_\varphi = \cos\varphi$, and $t_\varphi = \tan\varphi$. The position vectors $\boldsymbol{B}_i$ of B_i on B in $\{B\}$, the position vectors ${}^m\mathbf{b}_i$ of b_i on m in $\{m\}$, the position vectors $\boldsymbol{b}_i$ of b_i on m in $\{B\}$, and the position vector $\boldsymbol{o}$ of o on m in $\{B\}$, the unit vectors $\boldsymbol{\delta}_i$ of $\boldsymbol{r}_i$ and the vector $\boldsymbol{e}_i$ of the line e_i in $\{B\}$ can be expressed as follows: [23]

$$\boldsymbol{B}_i = \begin{pmatrix} X_{Bi} \\ Y_{Bi} \\ Z_{Bi} \end{pmatrix}, {}^m\boldsymbol{b}_i = \begin{pmatrix} x_{bi} \\ y_{bi} \\ z_{bi} \end{pmatrix}, \boldsymbol{b}_i = \begin{pmatrix} X_{bi} \\ Y_{bi} \\ Z_{bi} \end{pmatrix},$$
$$\boldsymbol{o} = \begin{pmatrix} X_o \\ Y_o \\ Z_o \end{pmatrix}, {}^B_m\boldsymbol{R} = \begin{pmatrix} x_l & y_l & z_l \\ x_m & y_m & z_m \\ x_n & y_n & z_n \end{pmatrix},$$
$$\boldsymbol{b}_i = {}^B_m\boldsymbol{R}\,{}^m\boldsymbol{b}_i + \boldsymbol{o},\ r_i = \left|\boldsymbol{b}_i - \boldsymbol{B}_i\right|,\ \boldsymbol{\delta}_i = \frac{\boldsymbol{b}_i - \boldsymbol{B}_i}{r_i},\ \boldsymbol{e}_i = \boldsymbol{b}_i - \boldsymbol{o}. \tag{1}$$

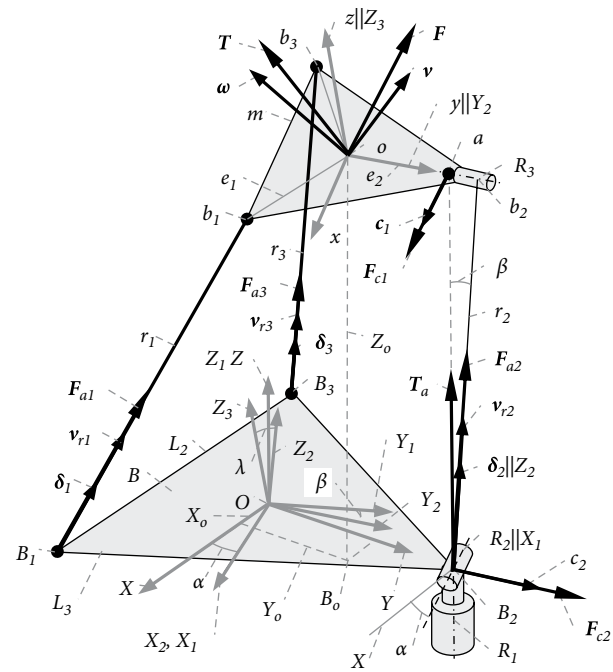

Figure 2: Kinematics and statics model of 2SPS+RRPR PM.

here, (X_o, Y_o, Z_o) are the components of $\boldsymbol{o}$ in $\{B\}$; ${}^B_m\boldsymbol{R}$ is a rotational transformation matrix from $\{m\}$ to $\{B\}$; $(x_l, x_m, x_n, y_l, y_m, y_n, z_l, z_m, z_n)$ are nine orientation parameters of m.

The formulas for solving ${}^m\boldsymbol{b}_i$ $(i = 1, 2, 3)$, $\boldsymbol{b}_i$ and $\boldsymbol{B}_i$ are derived from Equation (1) and represented as follows:

$$ {}^m\boldsymbol{b}_i = \frac{e}{2}\begin{pmatrix} \pm q \\ -1 \\ 0 \end{pmatrix}, {}^m\boldsymbol{b}_2 = \begin{pmatrix} 0 \\ e \\ 0 \end{pmatrix}, \boldsymbol{B}_i = \frac{E}{2}\begin{pmatrix} \pm q \\ -1 \\ 0 \end{pmatrix}, \boldsymbol{B}_2 = \begin{pmatrix} 0 \\ E \\ 0 \end{pmatrix},$$
$$\boldsymbol{b}_i = \frac{1}{2}\begin{pmatrix} \pm q e x_l - e y_l + 2X_o \\ \pm q e x_m - e y_m + 2Y_o \\ \pm q e x_n - e y_n + 2Z_o \end{pmatrix}, \boldsymbol{b}_2 = \begin{pmatrix} e y_l + X_o \\ e y_m + Y_o \\ e y_n + Z_o \end{pmatrix},$$
$$q = \sqrt{3};\ i = 1, \pm = +;\ i = 3, \pm = - \tag{2}$$

here, e is the distance from b_i to o, E is the distance from B_i to O.

Under the geometric constraints of the RRPR-type constraining active leg r_2, ${}^B_m\boldsymbol{R}$ is formed by 3 rotations of (Z, X_1, Y_2), namely, a rotation of α about Z-axis i.e., R_1, followed by a rotation of β about X_1-axis i.e., R_2, and a rotation of λ about Y_2-axis i.e., R_3. Here, X_1 is formed by X rotating about Z by α, and Y_2 is formed by Y_1 rotating about X_1 by β, see Figure 2. Each of $(x_l, x_m, x_n, y_l, y_m, y_n, X_o, Y_o)$ can be expressed by (α, β, λ) from Equations (1) and (2) as follows:

$$x_l = c_\alpha c_\lambda - s_\alpha s_\beta s_\lambda,\ x_m = s_\alpha c_\lambda + c_\alpha s_\beta s_\lambda,\ x_n = -c_\beta s_\lambda,$$
$$y_l = -s_\alpha c_\beta,\ y_m = c_\alpha c_\beta,\ y_n = s_\beta,$$
$$X_o = -\frac{y_l(e + Z_o y_n)}{y_l^2 + y_m^2} = \frac{s_\alpha}{c_\beta}\left(e + Z_o s_\beta\right),$$
$$Y_o = E - \frac{y_m(e + Z_o y_n)}{y_l^2 + y_m^2} = E - \frac{c_\alpha}{c_\beta}\left(e + Z_o s_\beta\right). \tag{3}$$

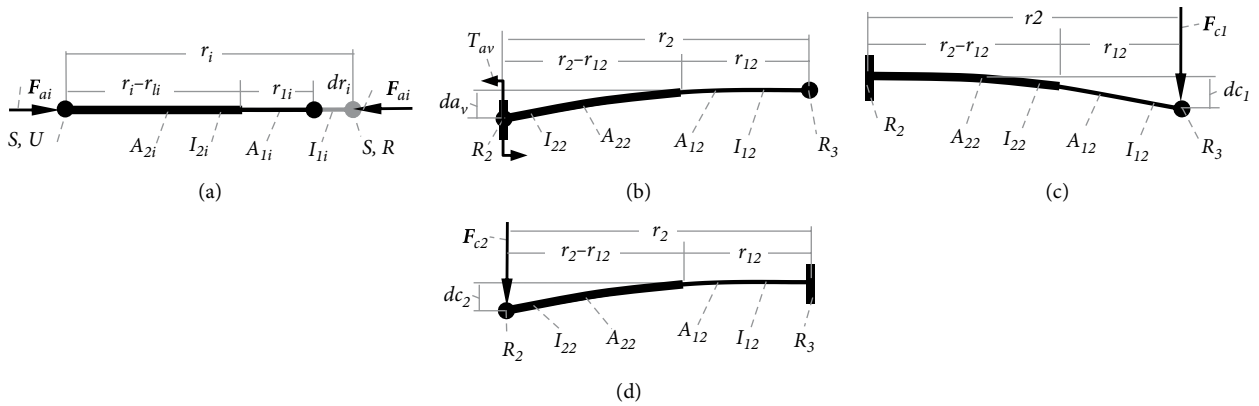

Figure 3: Elastic deformations of SPS-type legs and RRPR-type leg under $\boldsymbol{F}_{ai}$, $\boldsymbol{F}_{cj}$, and $\boldsymbol{T}_{cv}$.

$\boldsymbol{\delta}_i$, $\boldsymbol{e}_i$, $\boldsymbol{o}$, and r_i can be expressed by $(\alpha, \beta, \lambda, Z_o)$ from Equation (1) to Equation (3) as follows:

$$\boldsymbol{\delta}_i = \frac{1}{2r_1}\begin{pmatrix} \pm qe\left(c_\alpha c_\lambda - s_\alpha s_\beta s_\lambda\right) + es_\alpha c_\beta - \pm qE + 2\left(e + Z_o s_\beta\right)s_\alpha / c_\beta \\ \pm qe\left(s_\alpha c_\lambda + c_\alpha s_\beta s_\lambda\right) - ec_\alpha c_\beta + 3E - 2\left(e + Z_o s_\beta\right)c_\alpha / c_\beta \\ -\pm qec_\beta s_\lambda - es_\beta + 2Z_o \end{pmatrix},$$

$$\boldsymbol{\delta}_2 = \boldsymbol{Z}_2 = \begin{pmatrix} c_\alpha & -s_\alpha & 0 \\ s_\alpha & c_\alpha & 0 \\ 0 & 0 & 1 \end{pmatrix}\begin{pmatrix} 1 & 0 & 0 \\ 0 & c_\beta & -s_\beta \\ 0 & s_\beta & c_\beta \end{pmatrix}\begin{pmatrix} 0 \\ 0 \\ 1 \end{pmatrix} = \begin{pmatrix} s_\alpha s_\beta \\ -c_\alpha s_\beta \\ c_\beta \end{pmatrix}, \quad \begin{matrix} q = \sqrt{3}, \\ i = 1, \pm = +, \\ i = 3, \pm = -, \end{matrix}$$

$$\boldsymbol{e}_i = \frac{e}{2}\begin{pmatrix} \pm q\left(c_\alpha c_\lambda - s_\alpha s_\beta s_\lambda\right) + s_\alpha c_\beta \\ \pm q\left(s_\alpha c_\lambda + c_\alpha s_\beta s_\lambda\right) - c_\alpha c_\beta \\ -qc_\beta c_\lambda - s_\beta \end{pmatrix},$$

$$\boldsymbol{e}_2 = e\begin{pmatrix} -s_\alpha c_\beta \\ c_\alpha c_\beta \\ s_\beta \end{pmatrix}, \boldsymbol{o} = \begin{pmatrix} \left(e + Z_o s_\beta\right)s_\alpha / c_\beta \\ E - \left(e + Z_o s_\beta\right)c_\alpha / c_\beta \\ Z_o \end{pmatrix},$$

$$r_i^2 = \frac{D + 2e^2 + EY_o \pm q\left(eD_1 - EX_o\right) + eE\left(\pm qy_l \pm qx_m - 3x_l - y_m\right)}{2},$$

$$r_2^2 = D - e^2 - 2E\left(ey_m + Y_o\right), D = X_o^2 + Y_o^2 + Z_o^2 + E^2,$$

$$D_1 = x_l X_o + x_m Y_o + x_n Z_o. \tag{4}$$

The force situation of the 2SPS + RRPR PM is shown in Figure 2. The whole workloads can be simplified as a wrench $(\boldsymbol{F}, \boldsymbol{T})$ applied onto m at o. Here, $\boldsymbol{F}$ is a concentrated force and $\boldsymbol{T}$ is a concentrated torque. $(\boldsymbol{F}, \boldsymbol{T})$ includes the inertia wrench and the gravity of m, and inertia wrench and the gravity of the active legs and the external working wrench.

After solving the kinematics of the general PM and its legs, $(\boldsymbol{F}, \boldsymbol{T})$ can be solved [23]. $(\boldsymbol{F}, \boldsymbol{T})$ are balanced by 3 active forces $\boldsymbol{F}_{ai}(i = 1, 2, 3)$, an active torque $\boldsymbol{T}_a$, and 2 constrained forces $\boldsymbol{F}_{cj}(j = 1, 2)$. Here, each of $\boldsymbol{F}_{ai}$ due to the linear actuators is applied on and along r_i at B_i, its unit vector $\boldsymbol{\delta}_i$ is the same as that of r_i; $\boldsymbol{T}_a$ due to the motor 1 is applied on r_2 at B_2 and coincident with R_1.

Let $\boldsymbol{c}_j$ be the unit vector of $\boldsymbol{F}_{cj}$, $\boldsymbol{d}_j$ be the arm vector from $\boldsymbol{F}_{cj}$ to o. Let $\boldsymbol{v}$ and $\boldsymbol{\omega}$ be the translational and angular velocities. Since $\boldsymbol{F}_{cj}(j = 1, 2)$ limits the movement of PMs, based on principle of virtual work in [23], it is known that $\boldsymbol{F}_{cj}(j = 1, 2)$ does not produce any power. Thus, there are

$$F_{cj}\boldsymbol{c}_j \cdot \boldsymbol{v} + \left(\boldsymbol{d}_j \times F_{cj}\boldsymbol{c}_j\right) \cdot \boldsymbol{\omega} = 0 \quad \begin{matrix} \\ j = 1,\ 2 \end{matrix} \Rightarrow \begin{pmatrix} 0 \\ 0 \end{pmatrix} = \begin{pmatrix} \boldsymbol{c}_1 & \left(\boldsymbol{d}_1 \times \boldsymbol{c}_1\right)^T \\ \boldsymbol{c}_2 & \left(\boldsymbol{d}_2 \times \boldsymbol{c}_2\right)^T \end{pmatrix}\begin{pmatrix} \boldsymbol{v} \\ \boldsymbol{\omega} \end{pmatrix}. \tag{5}$$

Thus, the geometric constrains of $\boldsymbol{F}_{cj}(j = 1, 2)$ are determined in [23] as follows:

(1) Let $\boldsymbol{v}_{r2}$ be a velocity along prismatic joint P in r_2, $\boldsymbol{F}_{cj}\boldsymbol{v}_{r2} = 0$ i.e., $\boldsymbol{F}_{cj} \perp r_2$ must be satisfied.

(2) Let $\boldsymbol{R}_i(i = 1, 2, 3)$ be a unit vector of revolute joints R_i in r_2. Let $\boldsymbol{\rho}_r \times \boldsymbol{F}_{cj}$ be a torque of $\boldsymbol{F}_{cj}$ about R_i, $\boldsymbol{R}_i \cdot \left(\boldsymbol{\rho}_r \times \boldsymbol{F}_{cj}\right) = 0$ must be satisfied. Thus, each of $\boldsymbol{F}_{cj}$ must either intersect or be parallel with all the revolute joints R_i in r_2. Thus, the geometric constrained conditions $\{\boldsymbol{F}_{c1} || R_2$, $\boldsymbol{F}_{c1}$ intersecting with both R_1 and R_3 at point a, $\boldsymbol{F}_{c2} || R_3$, $\boldsymbol{F}_{c2}$ intersecting with both R_1 and R_2 at point $B_2\}$ are satisfied.

From the geometric constrains of $\boldsymbol{F}_{cj}(j = 1, 2)$, it leads to

$$\boldsymbol{c}_1 = \boldsymbol{R}_2 = \begin{pmatrix} c_\alpha \\ s_\alpha \\ 0 \end{pmatrix}, \boldsymbol{c}_2 = \boldsymbol{R}_3 = \begin{pmatrix} -s_\alpha c_\beta \\ c_\alpha c_\beta \\ s_\beta \end{pmatrix}, \boldsymbol{a} = \begin{pmatrix} 0 \\ E \\ \frac{Z_o + \left(e + Z_o s_\beta\right)t_\beta}{c_\beta} \end{pmatrix},$$

$$\boldsymbol{a} - \boldsymbol{b}_2 = t_\beta\left(es_\beta + Z_o\right)\begin{pmatrix} -s_\alpha \\ c_\alpha \\ t_\beta \end{pmatrix}, \boldsymbol{d}_1 = \boldsymbol{a} - \boldsymbol{o} = \frac{\left(e + Z_o s_\beta\right)}{c_\beta}\begin{pmatrix} -s_\alpha \\ c_\alpha \\ t_\beta \end{pmatrix},$$

$$\boldsymbol{d}_2 = \boldsymbol{B}_2 - \boldsymbol{o} = \frac{1}{c_\beta}\begin{pmatrix} -s_\alpha\left(e + Z_o s_\beta\right) \\ c_\alpha\left(e + Z_o s_\beta\right) \\ -Z_o c_\beta \end{pmatrix}. \tag{6}$$

The general input velocity $\boldsymbol{V}_r$, the general output velocity $\boldsymbol{V}$ in $\{B\}$, $F_{ai}(i = 1, 2, 3)$, T_a and $F_{cj}(j = 1, 2)$ have been derived based on Equations (4)–(6) as follows:

$$\boldsymbol{V}_r = \boldsymbol{J}_{6\times6}\boldsymbol{V}, \boldsymbol{V} = \boldsymbol{J}^{-1}\boldsymbol{V}_r, \alpha' = (\boldsymbol{0}_{1\times3} \quad \boldsymbol{s}^T)\boldsymbol{V},$$
$$\boldsymbol{V} = \begin{pmatrix} \boldsymbol{v} \\ \boldsymbol{\omega} \end{pmatrix}, \boldsymbol{s} = \begin{pmatrix} s_\alpha t_\beta \\ -c_\alpha t_\beta \\ 1 \end{pmatrix}, \boldsymbol{V}_r = \begin{pmatrix} v_{r1} \\ v_{r2} \\ v_{r3} \\ \alpha' \\ 0 \\ 0 \end{pmatrix},$$
$$\boldsymbol{F} = \begin{pmatrix} F_x \\ F_y \\ F_z \end{pmatrix}, \boldsymbol{T} = \begin{pmatrix} T_x \\ T_y \\ T_z \end{pmatrix},$$
$$\boldsymbol{J} = \begin{pmatrix} \boldsymbol{\delta}_1^T & (\boldsymbol{e}_1 \times \boldsymbol{\delta}_1)^T \\ \boldsymbol{\delta}_2^T & (\boldsymbol{e}_2 \times \boldsymbol{\delta}_2)^T \\ \boldsymbol{\delta}_3^T & (\boldsymbol{e}_3 \times \boldsymbol{\delta}_3)^T \\ \boldsymbol{0}_{1\times3} & \boldsymbol{s}^T \\ \boldsymbol{c}_1^T & (\boldsymbol{d}_1 \times \boldsymbol{c}_1)^T \\ \boldsymbol{c}_2^T & (\boldsymbol{d}_2 \times \boldsymbol{c}_2)^T \end{pmatrix}, \begin{pmatrix} F_{a1} \\ F_{a2} \\ F_{a3} \\ T_a \\ F_{c1} \\ F_{c2} \end{pmatrix} = -\left(\boldsymbol{J}^T\right)^{-1}\begin{pmatrix} \boldsymbol{F} \\ \boldsymbol{T} \end{pmatrix} \tag{7}$$

here, $\boldsymbol{J}$ is a 6×6 Jacobian matrix of the 2SPS+RRPR PM, α' is an angular velocity of R_1 (motor 1).

3. Stiffness Matrix and Elastic Deformation of SPS-Type Legs and RRPR-Type Leg

Suppose that the rigid platform m is elastically suspended and by 3 elastic active legs r_i and is constrained by one elastic constrained leg r_2. If only small displacements from its unpreloaded equilibrium position are considered, the overall wrench–deflection relation of the mechanism is linear elasticity. Based on the constructed workspace, each of length of piston/cylinder for active legs and constrained leg can be determined. Let r_{1i}, A_{1i}, I_{1i} and J_{1i} be the length, the section of a piston, the moment of inertia, and the rotational moment of inertia of leg r_i, respectively. Let $(r_i - r_{1i})$, A_{2i}, I_{2i}, and J_{2i} be the length, the section, the moment of inertia, and the rotational moment of inertia of a cylinder of r_i, respectively. Let E_{li} and G_i be the modulus of elasticity and the rotational modulus of elasticity for leg r_i, $(i = 1, 2, 3)$. When each of the active forces $\boldsymbol{F}_{ai}(i = 1, 2, 3)$ applies onto the SPS-type active leg $r_i\,(i = 1, 3)$ and the RRPR-type constrained active leg $r_i(i = 2)$ and along r_i, the longitudinal elastic differential deformation dr_i of leg r_i, see Figure 3(a).

The longitudinal elastic differential deformations of the SPS-type active leg $r_i(i = 1, 3)$ and the RRPR-type composite active leg $r_i(i = 2)$ under $\boldsymbol{F}_{ai}$ (a), The transverse elastic differential deformations of the RRPR-type composite leg r_2 under $\boldsymbol{F}_{cj}$ (b, c) and $\boldsymbol{T}_{cv}$ (d).

When each of the active forces $\boldsymbol{F}_{ai}(i = 1, 2, 3)$ applies onto the SPS-type active leg $r_i(i = 1, 3)$ and the RRPR-type constrained active leg $r_i(i = 2)$ and along r_i, the longitudinal elastic differential deformation dr_i of leg r_i (see Figure 3(a)) can be solved as below [24]

$$dr_i = \frac{F_{ai}}{k_{ai}},\ F_{ai} = k_{ai}dr_i,\ k_{ai} = -\frac{E_i}{\left(\frac{r_i - r_{1i}}{A_{2i}}\right) + \left(\frac{r_{1i}}{A_{1i}}\right)}, \tag{8}$$

here, k_{ai} is a longitudinal stiffness of SPS active leg r_i and RRPR-type constrained active leg $r_i(i = 2)$.

The active torque $\boldsymbol{T}_a$ consists of a component $\boldsymbol{T}_{au}$ along r_2 and a component $\boldsymbol{T}_{av}$ perpendicular to r_2 (see Figure 3(b)). They can be expressed as follows:

$$\boldsymbol{T}_a = T_a\boldsymbol{Z},\ T_{au} = \boldsymbol{T}_a \cdot \boldsymbol{\delta}_2 = T_a c_\beta,\ T_{av} = T_a\boldsymbol{Z} \cdot (\boldsymbol{\delta}_2 \times \boldsymbol{R}_2) = T_a s_\beta. \tag{9}$$

When T_{av} is exerted onto leg r_2 at universal joint and $T_{av} \perp r_2$ is satisfied, the transverse elastic differential deflection da_v of r_2 at its end (Figure 3(b)) can be solved in [24] as follows:

$$da_v = -\frac{T_{av}}{2E_2}\left[\frac{r_{12}^2}{I_{12}} + \frac{(r_2 - r_{12})^2}{I_{22}}\right] = \frac{T_a}{k_{av}},$$
$$k_{av} = \frac{-2E_2}{\left[\left(\frac{r_{12}^2}{I_{12}}\right)s_\beta + \left(\frac{(r_2 - r_{12})^2}{I_{22}}\right)s_\beta\right]}. \tag{10}$$

When T_{au} is exerted onto leg r_2 at universal joint, the elastic rotational differential deformation $d\theta_1$ of leg r_2 at its end can be solved based on the elastic deformation formula in [24] as below

$$d\theta_1 = -\frac{T_{au}}{G_2}\left(\frac{r_{12}}{J_{12}} + \frac{r_2 - r_{12}}{J_{22}}\right) = \frac{T_a}{k_{\theta1}},\ k_{\theta1} = \frac{-G_2}{\left(\left(\frac{r_{12}}{J_{12}}\right)c_\beta + \left(\frac{r_2 - r_{12}}{J_{22}}\right)c_\beta\right)}, \tag{11}$$

here, k_{av} and $k_{\theta1}$ are the transverse and rotational stiffness of leg r_2 vs. T_{av} and T_{au}, respectively.

From Equations (10)–(12), it leads to

$$da_v + d\theta_1 = \left(\frac{1}{k_{av}} + \frac{1}{k_{\theta1}}\right)T_a, \rightarrow T_a = k_1(da_v + d\theta_1),$$
$$k_1 = \frac{1}{\left(\frac{1}{k_{av}}\right) + \left(\frac{1}{k_{\theta1}}\right)}. \tag{12}$$

When $\boldsymbol{F}_{c1}$ is exerted onto leg r_2 at point a and $F_{c1}\ r_2$ is satisfied, the transverse elastic differential deflection dc_1 of r_2 at its end (see Figure 3(c)) can be solved [24] as follows:

$$dc_1 = \frac{F_{c1}}{k_{c1}},\ k_{c1} = \frac{-3E_2}{\left[r_{12}^3/I_{12}\right] + \left[(r_2 - r_{12})\left(r_2^2 + r_{12}^2 + r_2 r_{12}\right)/I_{22}\right]}, \tag{13}$$

here k_{c1} is a transverse stiffness of r_2 vs. F_{c1}.

When $\boldsymbol{F}_{c1}$ is exerted onto leg r_2 at point a and $F_{c1}\ r_2$ is satisfied, the elastic rotational differential deformation $d\theta_2$ of leg r_2 at its end can be solved in [24] as follows:

$$d\theta_2 = \frac{|a - b_2|F_{c1}}{G_2}\left[\left(\frac{r_2 - r_{12}}{I_{22}} + \frac{r_{12}}{I_{12}}\right)\right] = \frac{F_{c1}}{k_{\theta2}},$$
$$k_{\theta2} = \frac{G_2}{\left[|a - b_2|\left((r_2 - r_{12}/I_{22}) + (r_{12}/I_{12})\right)\right]}. \tag{14}$$

Similarly, from Equations (15) and (16), it leads to

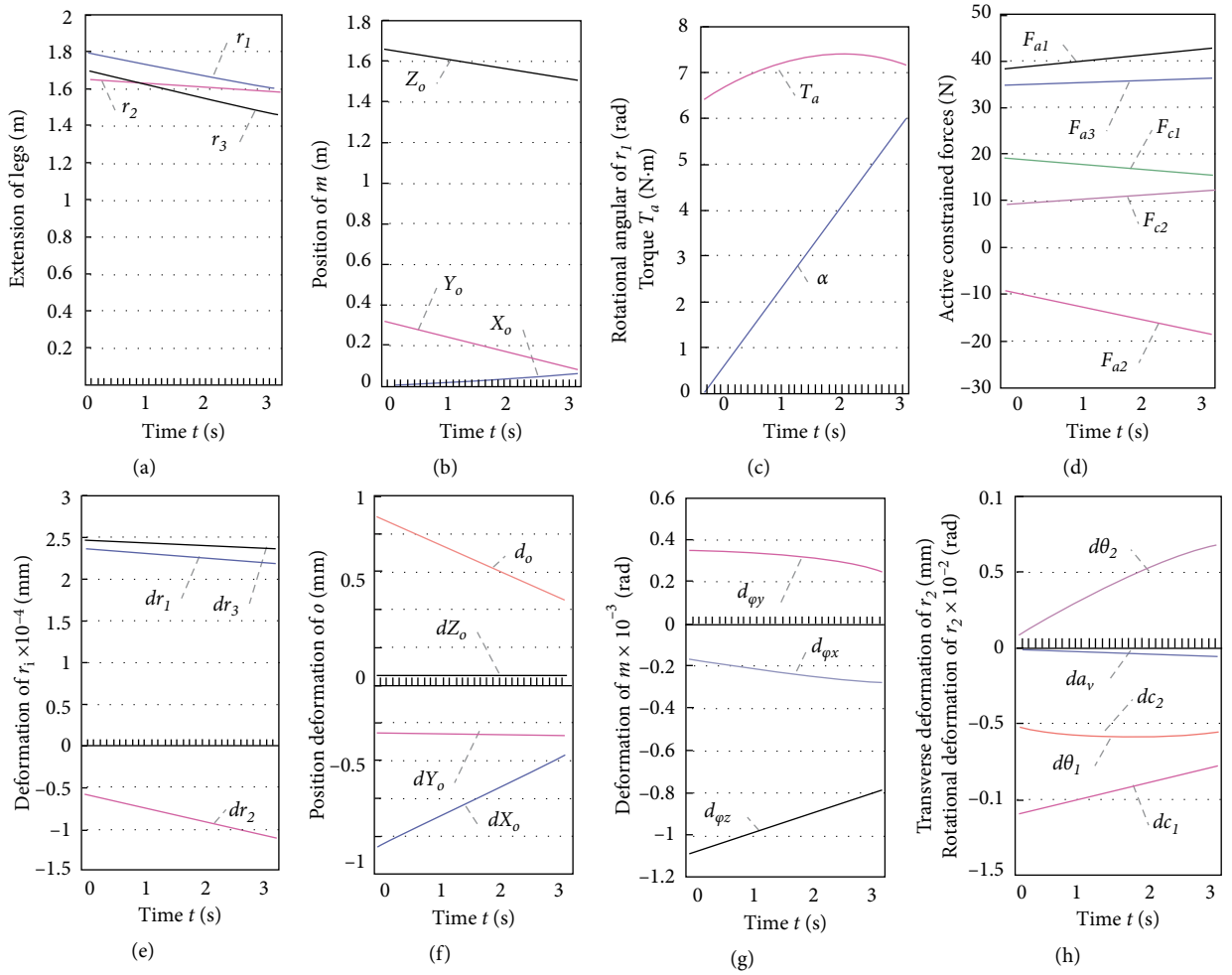

Figure 4: Theoretical solutions of elastic deformations of 2SPS + RRPR PM.

$$dc_1 + d\theta_2 = \left(\frac{1}{k_{c1}} + \frac{1}{k_{\theta 2}}\right)F_{c1}, \rightarrow F_{c1} = k_2(dc_1 + d\theta_2),$$
$$k_2 = \frac{1}{\left(\frac{1}{k_{c1}} + \frac{1}{k_{\theta 2}}\right)}. \tag{15}$$

When $\boldsymbol{F}_{c2}$ is exerted onto leg r_2 at B_2 and $F_{c2}\, r_2$ is satisfied, the transverse elastic differential deflection dc_2 of r_2 at its end (see Figure 3(d)) can be solved in [24] as follows:

$$dc_2 = \frac{F_{c2}}{k_{c2}},\ k_{c2} = \frac{-3E_2}{\left[\left((r_2 - r_{12})^3/I_{22}\right) + \left(r_{12}^3 + 3(r_2 - r_{12})r_2 r_{12}/I_{12}\right)\right]}. \tag{16}$$

Since $da_v | dc_1$ is satisfied, both $d\theta_1$ and $d\theta_2$ are the elastic rotational differential deformations of r_2, an equation of force-deformation for the 2SPS + RRPR PM is derived from Equation (8) to Equation (16) as follows:

here, $\boldsymbol{K}_r$ is a 6×6 symmetric total stiffness matrix of the legs $r_i (i = 1, 2, 3)$.

4. Total Stiffness Matrix and the Elastic Deformation of 2SPS+RRPR PM

Based on principle of virtual work in [22], it is known that when a deformed mechanical system keeps a static balance under all external wrenches, the sum of the work generated by all external wrenches along virtual displacements of the mechanical system and the work produced by all internal wrenches along virtual deformations of the same mechanical system must be zero. Therefore, the sum of the work generated by $(\boldsymbol{F}_{a1}, \boldsymbol{F}_{a2}, \boldsymbol{F}_{a3}, \boldsymbol{T}_a, \boldsymbol{F}_{c1}, \boldsymbol{F}_{c2})$ along deformations of the 2SPS + RRPR PM and the work produced by $(\boldsymbol{F}, \boldsymbol{T})$ along

$$\begin{pmatrix} F_{a1} \\ F_{a2} \\ F_{a3} \\ T_a \\ F_{c1} \\ F_{c2} \end{pmatrix} = \boldsymbol{K}_r \begin{pmatrix} dr_1 \\ dr_2 \\ dr_3 \\ dc \\ d\theta \\ dc_2 \end{pmatrix}, \begin{pmatrix} dr_1 \\ dr_2 \\ dr_3 \\ dc \\ d\theta \\ dc_2 \end{pmatrix} = \boldsymbol{K}_r^{-1} \begin{pmatrix} F_{a1} \\ F_{a2} \\ F_{a3} \\ T_a \\ F_{c1} \\ F_{c2} \end{pmatrix}, \boldsymbol{K}_r = \begin{pmatrix} k_{a1} & 0 & 0 & 0 & 0 & 0 \\ 0 & k_{a2} & 0 & 0 & 0 & 0 \\ 0 & 0 & k_{a3} & 0 & 0 & 0 \\ 0 & 0 & 0 & k_1 & 0 & 0 \\ 0 & 0 & 0 & 0 & k_2 & 0 \\ 0 & 0 & 0 & 0 & 0 & k_{c2} \end{pmatrix} \tag{17}$$
$$dc = da_v + dc_1, d\theta = d\theta_1 + d\theta_2, k_1 = \frac{1}{(1/k_{av}) + (1/k_{\theta 1})}, k_2 = \frac{1}{(1/k_{c1}) + (1/k_{\theta 2})}.$$

the displacements of point o in $\{B\}$ must be zero. Let (dX_o, dY_o, dZ_o) be 3 translational components of the elastic differential deformation of m at o in $\{B\}$; $(d\varphi_x, d\varphi_y, d\varphi_z)$ be 3 rotational components of the elastic differential deformation of m in $\{B\}$. Thus, based on the theorem of work and energy equal to each other, from Equation (7) to Equation (17), it leads to

$$\begin{pmatrix} dr_1 \\ dr_2 \\ dr_3 \\ dc \\ d\theta \\ dc_2 \end{pmatrix}^T \begin{pmatrix} F_{a1} \\ F_{a2} \\ F_{a3} \\ T_a \\ F_{c1} \\ F_{c2} \end{pmatrix} = -\begin{pmatrix} dX_o \\ dY_o \\ dZ_o \\ d\varphi_x \\ d\varphi_y \\ d\varphi_z \end{pmatrix}^T \begin{pmatrix} \boldsymbol{F} \\ \boldsymbol{T} \end{pmatrix}$$

$$\Rightarrow \begin{pmatrix} dr_1 \\ dr_2 \\ dr_3 \\ dc \\ d\theta \\ dc_2 \end{pmatrix}^T \left[-\left(\boldsymbol{J}^T\right)^{-1}\right] = -\begin{pmatrix} dX_o \\ dY_o \\ dZ_o \\ d\varphi_x \\ d\varphi_y \\ d\varphi_z \end{pmatrix}^T,$$

$$\begin{pmatrix} dr_1 \\ dr_2 \\ dr_3 \\ dc \\ d\theta \\ dc_2 \end{pmatrix}^T \left(\boldsymbol{J}^{-1}\right)^T = \begin{pmatrix} dX_o \\ dY_o \\ dZ_o \\ d\varphi_x \\ d\varphi_y \\ d\varphi_z \end{pmatrix}^T \Rightarrow \boldsymbol{J}^{-1} \begin{pmatrix} dr_1 \\ dr_2 \\ dr_3 \\ dc \\ d\theta \\ dc_2 \end{pmatrix}$$

$$= \begin{pmatrix} dX_o \\ dY_o \\ dZ_o \\ d\varphi_x \\ d\varphi_y \\ d\varphi_z \end{pmatrix} \Rightarrow \begin{pmatrix} dr_1 \\ dr_2 \\ dr_3 \\ dc \\ d\theta \\ dc_2 \end{pmatrix} = \boldsymbol{J} \begin{pmatrix} dX_o \\ dY_o \\ dZ_o \\ d\varphi_x \\ d\varphi_y \\ d\varphi_z \end{pmatrix}. \tag{18}$$

Thus, from Equations (7), (14), and (15), it leads to

$$\begin{pmatrix} dX_o \\ dY_o \\ dZ_o \\ d\varphi_x \\ d\varphi_y \\ d\varphi_z \end{pmatrix} = \boldsymbol{J}^{-1} \begin{pmatrix} dr_1 \\ dr_2 \\ dr_3 \\ dc \\ d\theta \\ dc_2 \end{pmatrix} \Rightarrow \begin{pmatrix} dX_o \\ dY_o \\ dZ_o \\ d\varphi_x \\ d\varphi_y \\ d\varphi_z \end{pmatrix}$$

$$= \boldsymbol{J}^{-1}\boldsymbol{K}_r^{-1} \begin{pmatrix} F_{a1} \\ F_{a2} \\ F_{a3} \\ T_a \\ F_{c1} \\ F_{c2} \end{pmatrix}, \begin{pmatrix} F_{a1} \\ F_{a2} \\ F_{a3} \\ T_a \\ F_{c1} \\ F_{c2} \end{pmatrix}$$

$$= -\left(\boldsymbol{J}^T\right)^{-1} \begin{pmatrix} \boldsymbol{F} \\ \boldsymbol{T} \end{pmatrix}, \Rightarrow \begin{pmatrix} dX_o \\ dY_o \\ dZ_o \\ d\varphi_x \\ d\varphi_y \\ d\varphi_z \end{pmatrix} = \boldsymbol{K}^{-1} \begin{pmatrix} \boldsymbol{F} \\ \boldsymbol{T} \end{pmatrix} \Rightarrow \boldsymbol{K}^{-1}$$

$$= -\boldsymbol{J}^{-1}\boldsymbol{K}_r^{-1}\left(\boldsymbol{J}^T\right)^{-1} \Rightarrow \begin{pmatrix} \boldsymbol{F} \\ \boldsymbol{T} \end{pmatrix} = \boldsymbol{K} \begin{pmatrix} dX_o \\ dY_o \\ dZ_o \\ d\varphi_x \\ d\varphi_y \\ d\varphi_z \end{pmatrix}, \tag{19}$$

Here

$$\boldsymbol{K} = -\left[\boldsymbol{J}^{-1}\boldsymbol{K}_r^{-1}\left(\boldsymbol{J}^T\right)^{-1}\right]^{-1}$$

$$= -\left(\boldsymbol{J}^T\boldsymbol{K}_r\boldsymbol{J}\right)_{6\times 6} = \begin{pmatrix} k_{11} & k_{12} & \cdots & k_{16} \\ k_{21} & k_{22} & \cdots & k_{26} \\ \vdots & \vdots & \vdots & \vdots \\ k_{61} & k_{62} & \cdots & k_{66} \end{pmatrix}, \tag{20}$$

here $\boldsymbol{K}$ is a 6×6 symmetric total stiffness matrix of this manipulator; $(dX_o, dY_o, dZ_o, d\varphi_x, d\varphi_y, d\varphi_z)$ are the 6 elastic deformation components of platform. When given $(\boldsymbol{F}, \boldsymbol{T})$, the elastic differential deformation of this manipulator can be solved from Equation (19).

5. Analytic Solved Example of Elastic Deformation for 2SPS+RRPR PM

In the 2SPS + RRPR type PM, let initial independent pose variables vary vs. time t when given pose parameters $(\alpha, \beta, \lambda, Z_o)$, see Figures 4(a) and 4(b).

Set $L = 1.2\,\text{m}$, $l = 0.6\,\text{m}$; $\boldsymbol{F} = -[20\ 30\ 60]^T\,\text{N}$ and $\boldsymbol{T} = [-0.3\ -0.31]^T\,\text{N m}$, $E_i = 2.11 \times 10^{11}\,\text{Pa}$, the diameter of piston and cylinder for active legs $r_i (i = 1, 2, 3)$ are $D_{i1} = D_{i2} = 0.04\,\text{m}$, $E_iI_{i1} = E_iI_{i2} = 26502\,\text{N}\cdot\text{m}^2$, $A_{i1} = A_{i2} = 0.0013\,\text{m}^2$. By using the relevant theoretical equations and Matlab, the extensions of r_i and α are solved, see Figure 4(a). The position components (X_o, Y_o, Z_o) of the moving platform m are solved, see Figure 4(b). Three active forces $F_{ai} (i = 1, 2, 3)$, one active torque T_a, two constrained forces F_{c1} and F_{c2} are solved, see Figures 4(c) and 4(d). The longitudinal deformations $dr_i (i = 1, 2, 3)$ of r_i are solved, see Figure 4(e). The position deformations of m at o are solved, see Figure 4(f). The angular deformations of m are solved, see Figure 4(g). The transverse deformations $dc_j (j = 1, 2)$ and $dc_2 + da_v$ and the rotational deformations $d\theta_1$ and $d\theta_2$ of r_2 are solved, see Figure 4(h).

When $r_1 = 1.8$, $r_3 = 1.7$, $r_2 = 1.66\,\text{m}$. $\alpha = 0$, $\boldsymbol{K}$ is solved from Equations (7) and (20) as follows:

$$K = \begin{pmatrix} 0.0923 & 0.0130 & 0.0266 & 0.0038 & 0.1466 & -0.0279 \\ 0.0130 & 0.2417 & 0.7799 & -0.1465 & 0.0052 & -0.0042 \\ 0.0266 & 0.7799 & 4.2941 & 0.0905 & -0.0097 & -0.0090 \\ 0.0038 & -0.1465 & 0.0905 & 0.2721 & 0.0150 & -0.0010 \\ 0.1466 & 0.0052 & -0.0097 & 0.0150 & 0.2338 & -0.0446 \\ -0.0279 & -0.0042 & -0.0090 & -0.0010 & -0.0446 & 0.0084 \end{pmatrix}. \tag{21}$$

6. A FE Model of 2SPS + RRPR PM and Its Solutions

A 3D assembly mechanism of the 2SPS + RRPR PM is constructed in SolidWorks [25]. Next, its finite element (FE) model is generated in ANSYS, see Figure 5. All relative geometry and material parameters of the 3D simulation assembly mechanism are the same as that in Section 5. The 3 equivalent revolute joints for 3 actuated revolute joints and 4 equivalent spherical joints for 4 actuated spherical joints are constructed, see Figure 5(a). The applied loads are shown in Figure 5(b). The boundary condition are explained as follows:

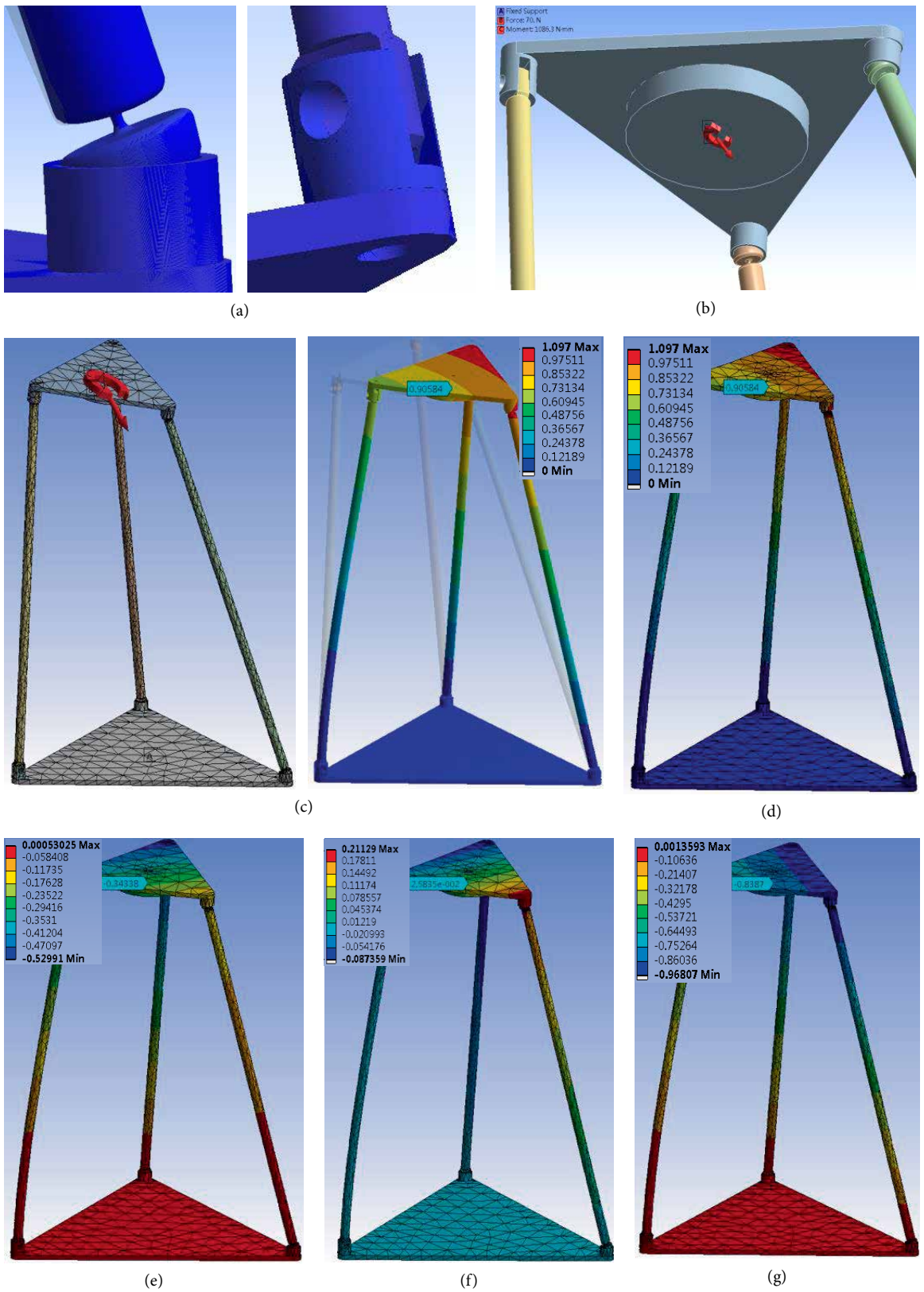

FIGURE 5: Simulation solutions of elastic deformations of EF model of the 2SPS + RRPR PM. (a) Equivalent spherical joint S and revolute joints R_1 and R_2, (b) load condition, (c) FE model of 2SPS + UPR PM and its elastic deformation, (d) elastic deformation of o, (e) elastic deformation dX_o, (f) elastic deformation dY_o and (g) elastic deformation dZ_o.

Table 1: Simulation solved results of elastic deformations of EF model of 2SPS + RRPR PM.

Elastic deformation of o, mm			Position of m (m)		
	FE model	Theoretical	X_o	Y_o	Z_o
do	0.9058	0.8934	FE model position of No. 19319 joint		
dX_o	−0.8387	−0.8550	−0.049	0.317	1.71
dY_o	−0.3434	−0.2547	Theoretical position of o		
dZ_o	0.0258	0.0534	0	0.3192	1.6540

(1) If no setting is given, all the assembly parts in the FE model may constitute the same elastic body. Therefore, each of the assembly spherical joints in FE model constitutes the same elastic body. The simulation 3D assembly of spherical joints is used only for varying the pose of PM and the workload applied on m at o.

(2) All the relative geometry parameters of the 3D simulation assembly mechanism are the same as that in Section 5. The material parameters of $r_i (i = 1, 2, 3)$ are set as the same as that in Section 5.

(3) Construct 3 equivalent spherical joints for 4 actuated spherical joints, see Figure 5(a). Here, the diameters at the two ends of the SPS-type legs $r_i (i = 1, 3)$ are reduced sharply.

(4) Construct 3 equivalent revolute joints for the actuated revolute joints R_1, R_2, R_3, see Figures 5(a) and 5(b). Here, two holes for each of equivalent revolute joints are constructed and kept coincident with each other; the rotational stiffness and the axial stiffness are set as 0 and 1×10^{10} N/mm, respectively, according to the requirement for revolute joint in software.

(5) Each of the 3 linear active legs with prismatic joints is formed using the elastic linear rod, which is assigned by the alloy steel. Set SPS leg $r_1 = 1.8$, SPS leg $r_3 = 1.7$, RRPR leg $r_2 = 1.66$ m.

(6) A fixed constraint is added onto the base, which is assigned by the alloy steel with rigid body.

(7) The workload wrench $\boldsymbol{F} = -[20\ 30\ 60]^T$N and $\boldsymbol{T} = [-0.3\ -\ 0.31]^T$N m are applied onto m at o, which is assigned by the alloy steel with the rigid body, see Figure 5(b).

Some solved results of the elastic deformations are shown in Figures 5(c)–5(g) and Table 1.

An existing CAD software provides a function for automatically optimal mesh in order to avoid singularity element and to obtain the suitable results of finite element analysis (FEM). Therefore, the 3D assembly mechanism of the 2SPS + RRPR PM is automatically meshed by the function for automatically optimal mesh.

7. Analysis of Stiffness and Elastic Deformation of 2SPS+RRPR PM

Several conclusions are obtained from theoretical and simulation solutions as follows:

(1) The solved results of FE model in most cases are approximate numerical results which depend on some key factors such as finite element dimension and type, equivalence between actual joints and simulation joints, selected material parameter, solver, reasonable boundary constraints and connection constraints [23].

(2) It is known from Table 1 that the elastic deformations of FE model of this PM are basically coincident with that of theoretical ones in Section 5.

(3) It is known from Figures 4(e) and 4(h) that the transverse elastic deformations $dc_j (j = 1, 2)$ $(0.5 \rightarrow 1.2 \times 10^{-4})$ of r_2 due to the constrained forces F_{cj} are greatly larger than the longitudinal elastic deformation dr_i $(0.5 \rightarrow 2.5 \times 10^{-7})$ of due to active forces F_{ai}. It implies that the constrained wrench has great influence on the elastic deformation of this PM.

(4) It is known from Figure 4(c), h that the transverse elastic deformations $dc_j (j = 1, 2)$ of r_2 due to the constrained forces F_{cj} is larger than the transverse elastic deformation da_v of r_2 due to active torque T_{av}. The transverse elastic deformations and elastic rotational deformation of the SPS-type legs $r_i (i = 1, 3)$ is 0. Therefore, the diameter of piston and cylinder of r_2 should be increased.

(5) It is known from Figure 4(h) that the elastic rotational deformation $d\theta_1$ of r_2 due to F_{c1} and the elastic rotational deformation $d\theta_2$ of r_2 due to F_{c2} are inversely proportional to each other.

8. Conclusions

A 2SPS + RRPR parallel manipulator with asymmetrical structure is suitable for the helicopter rotor supporting base.

The formulas for solving the stiffness matrix and the elastic deformation of its three asymmetrical legs are derived. The formulas for solving its total stiffness matrix and the elastic deformation are derived based on the Jacobian matrix and the stiffness matrix of three asymmetrical legs. Both the stiffness matrix of its three asymmetrical legs and its total stiffness matrix are 6×6 symmetric matrices, although this manipulator has asymmetrical structure.

The constrained wrench must be taken into account when establishing its total stiffness matrix and solving its elastic deformation.

The proposed methodological results can be applied to other less mobility parallel manipulators with asymmetrical structure and active legs for solving the elastic deformations of asymmetrical active legs and the elastic deformations of moving platform.

Nomenclatures

DoF: Degree of freedom
PM: Parallel manipulator
B, m: Base and moving platform
$\{m\}$: Coordinate frame o-xyz fixed on m
$\{B\}$: Coordinate frame O-XYZ fixed on B
o: The center point of m
O: The center point of B
b_jB_j: The vertices of m, $B(j = 1, 2, 3)$
l, L: The side of m, B
e: The distances from b_i to o
E: The distances from B_i to O
r_i: Active leg and its length $(i = 1, 2, 3)$
$R_1R_2R_3$: Three revolute joints
R, P: Revolute joint, prismatic joint
U, S: Universal joint and spherical joint
X_o, Y_o, Z_o: Position components of o in $\{B\}$
α, β, λ: Three Euler angles of m
${}^{B}_{m}\boldsymbol{R}$: Rotational transformation matrix
$\boldsymbol{J}$: Jacobian matrix
E_{li}: Modulus of elasticity for r_i
G_i: Rotational modulus of elasticity for r_i
$\boldsymbol{C}$: The total complacence matrix of PM
$\boldsymbol{T}_a$: The active torque
I_{ji}: Linear inertia moment of r_i
J_{ji}: Rotational inertia moment of r_i
$\boldsymbol{V}_r$: The general input velocity
$\boldsymbol{V}$: The general output velocity in $\{B\}$
x_l, x_m, x_n, y_l, y_m, y_n, z_l, z_m, z_n: Nine orientation parameters of ${}_{m}^{B}\boldsymbol{R}$
$\boldsymbol{v}_{ri}$: The input velocity along active leg r_i
$\boldsymbol{v}$, $\boldsymbol{\omega}$: The linear and angular velocities of m at o in $\{B\}$
$\boldsymbol{F}$, $\boldsymbol{T}$: The concentrated force and torque applied on m at o
$\boldsymbol{F}_{ai}$, $\boldsymbol{\delta}_i$: The active forces and their unit vectors
$\boldsymbol{F}_c$, $\boldsymbol{c}$: The constrained forces and their unit vectors
F_{au}, F_{av}: The components of $\boldsymbol{F}_{ai}$
F_{c1}, F_{c2}: The components of $\boldsymbol{F}_c$, $F_{c1}||r_2$, $F_{c2}\, r_2$
T_{au}, T_{av}: The components of $\boldsymbol{T}_a$, $T_{au}||r_2$, $T_{av}\, r_2$
$\boldsymbol{K}_r$: 6×6 total stiffness matrix of the legs $r_i(i = 1, 2, 3)$
k_{ai}: A longitudinal stiffness of r_i
k_{av}, $k_{\theta1}$: The transverse and rotational stiffness of leg r_2
k_{c1}: Transverse stiffness of r_2 in plane with F_{c1}
$\boldsymbol{K}$: The stiffness matrix of PM
dr_i: The longitudinal elastic differential deformation of leg r_i
dX_o, dY_o, dZ_o: 3 deformation components of m at o in $\{B\}$
$d\varphi_x$, $d\varphi_y$, $d\varphi_z$: 3 rotational deformation components of m in $\{B\}$
do: Elastic differential deformation of m at o in $\{B\}$
dc_2: Transverse elastic differential deflection of r_2 at its end
$d\theta_1$, $d\theta_2$: Rotational deformations of r_2
$d\alpha$, $d\beta$, $d\lambda$: Differential deformations of 3 Euler angles of m
φ: One of $(\alpha, \beta, \lambda, \gamma_1, \gamma_2)$, $s_\varphi = \sin\varphi$, $c_\varphi = \cos\varphi$, $t_\varphi = \tan\varphi$
r_{ij}: The length of r_i, $j = 1$ for piston, $j = 2$ for cylinder
A_{ji}, D_{ji}: The cross-section and the diameters of r_i
$||$, $\perp$, $|$: Perpendicular, parallel collinear constraint.

Data Availability

The data used to support the findings of this study are available from the corresponding author upon request.

Conflicts of Interest

The authors declare that they have no conflicts of interest.

Acknowledgments

The authors would like to acknowledge Major Research Project (91748125) supported by National Natural Science Foundation of China.

References

[1] R. Claudio, *Parallel Kinematic Machines*, Springer, London, UK, 2012.

[2] Z. Huang, Q. Li, and H. Ding, *Theory of Parallel Mechanisms*, Springer, New York, NY, USA, 2013.

[3] C. M. Gosselin and D. Zhang, "Stiffness analysis of parallel mechanisms using a lumped model," *International Journal of Robotics and Automation*, vol. 17, no. 1, pp. 17–27, 2002.

[4] D. Zhang and Y. T. Lang Sherman, "Stiffness modeling for a class of reconfigurable PKMs with three to five degrees of freedom," *Journal of Manufacturing Systems*, vol. 23, no. 4, pp. 316–327, 2004.

[5] C. Dong, H. Liu, and W. Yue, "Stiffness modeling and analysis of a novel 5-DOF hybrid robot," *Mechanism and Machine Theory*, vol. 125, no. 6, pp. 80–93, 2018.

[6] Y. M. Li and Q. Xu, "Stiffness analysis for a 3-PUU parallel kinematic machine," *Mechanism and Machine Theory*, vol. 43, no. 2, pp. 186–200, 2008.

[7] C. Yang, Q. Li, and Q. Chen, "Elastostatic stiffness modeling of overconstrained parallel manipulators," *Mechanism and Machine Theory*, vol. 122, no. 4, pp. 58–74, 2018.

[8] X. Zhou, Y. Xu, and J. Yao, "Stiffness modelling and comparison of the 5-UPS/PRPU parallel machine tool with its nonredundant counterpart," *Proceedings of the Institution of Mechanical Engineers, Part B: Journal of Engineering Manufacture*, vol. 231, no. 9, pp. 1646–1657, 2017.

[9] J. Enferadi and A. Tootoonchi, "Accuracy and stiffness analysis of a 3-RRP spherical parallel manipulator," *Robotica*, vol. 29, no. 2, pp. 193–209, 2011.

[10] A. Pashkevich, A. Klimchik, and D. Chablat, "Enhanced stiffness modeling of manipulators with passive joints," *Mechanism and Machine Theory*, vol. 46, no. 5, pp. 662–679, 2011.

[11] A. Pashkevich, D. Chablat, and P. Wenger, "Stiffness analysis of overconstrained parallel manipulators," *Mechanism and Machine Theory*, vol. 44, no. 5, pp. 966–982, 2009.

[12] T. Zhao, C. Wang, and X. Liu, "Stiffness and singularity analysis of foldable parallel mechanism for ship-based stabilized platform," *Robotica*, vol. 34, no. 4, pp. 913–924, 2016.

[13] Pham Huy-Hoang and I. M. Chen, "Stiffness modeling of flexure parallel mechanism," *Precision Engineering*, vol. 29, no. 4, pp. 467–478, 2005.

[14] G. Cheng, P. Xu, D. Yang, and H. Liu, "Stiffness analysis of a 3CPS parallel manipulator for mirror active adjusting platform in segmented telescope," *Robotics and Computer-Integrated Manufacturing*, vol. 29, no. 5, pp. 302–311, 2013.

[15] X. Shan and G. Cheng, "Static analysis on a 2(3PUS+S) parallel manipulator with two moving platforms," *Journal of Mechanical Science and Technology*, vol. 32, no. 8, pp. 3869–3876, 2018.

[16] G. Hao and X. Kong, "A normalization-based approach to the mobility analysis of spatial compliant multi-beam modules," *Mechanism and Machine Theory*, vol. 59, no. 1, pp. 1–19, 2013.

[17] Dan Wang, Rui Fan, and Wuyi Chen, "Stiffness analysis of a hexaglide parallel loading mechanism," *Mechanism and Machine Theory*, vol. 70, no. 12, pp. 454–473, 2013.

[18] Y. Lu and B. Hu, "Analysis of stiffness and elastic deformation for some 3~5-dof PKMs with SPR or RPS-type legs," *Journal of Mechanical Design*, vol. 130, no. 10, 2008.

[19] B. Hu, Y. Lu, Q. Tan, J. P. Yu, and J. Han, "Analysis of stiffness and elastic deformation of a 2(SP+SPR+SPU) serial-parallel manipulator," *Robotics and Computer-Integrated Manufacturing*, vol. 27, no. 2, pp. 418–425, 2011.

[20] B. Lian, T. Sun, and Y. Song, "Stiffness analysis and experiment of a novel 5-DoF parallel kinematic machine considering gravitational effects," *International Journal of Machine Tools & Manufacture*, vol. 95, no. 8, pp. 82–96, 2015.

[21] A. Klimchik, A. Pashkevich, and D. Chablat, "CAD-based approach for identification of elasto-static parameters of robotic manipulators," *Finite Elements in Analysis and Design*, vol. 75, no. 11, pp. 19–30, 2013.

[22] Y. G. Li, H. T. Liu, X. M. Zhao, T. Huang, and D. G. Chetwynd, "Design of a 3-DOF PKM module for large structural component machining," *Mechanism and Machine Theory*, vol. 45, no. 6, pp. 941–954, 2010.

[23] Y. Lu, B. Hu, and Y. Shi, "Kinematics analysis and statics of a 2SPS+UPR parallel manipulator," *Multibody System Dynamics*, vol. 18, no. 4, pp. 619–636, 2007.

[24] D. Roylance, *Mechanics of Material*, Joho Wiley & Sons Inc., New York, NY, USA, 1996.

[25] R. Chao, *Course of 3 Dimension Design and Application of Solidworks 2009*, China Machine Press, Beijing, China, 2nd edition, 2010.